Please cite as,

Kondou, C., Hrnjak, P.S., “Heat Rejection from R744 Flow under Uniform Temperature Cooling in a Horizontal Smooth Tube around the Critical Point”, Int. J. Refrig,. 34, 3, 719-731, (2011).

Title:

Heat rejection from R744 flow under uniform temperature cooling in a horizontal smooth tube around the critical point

Authors:

Chieko Kondou*[1], Pega Hrnjak[1,2]

Affiliations:

1, Department of Mechanical Science and Engineering, University of Illinois at Urbana-Champaign, 1206 West Green Street, Urbana, IL 61801, USA

2, Creative Thermal Solutions, 2209 North Willow Road, Urbana IL, 61802, USA

* Corresponding author.

Tel.: +1 217 333 8110

Fax: +1 217 333 1942

E-mail address: ckondo@uiuc.edu (C. Kondo)

Abstract:

Heat rejection from CO_2 flow near the critical point, where commercial refrigerators spend most of their operating hours, was investigated in this study. Experimental results on the heat transfer coefficient and pressure drop of mass flux from 100 to 240 kg $m^{-2}s^{-1}$ at pressures from 5 to 7.5 MPa in a horizontal smooth tube of 6.1 mm inner diameter are provided and compared with correlations. The heat rejection process below critical pressure was categorized into superheat, two-phase, and subcool zones in which the bulk-mean temperature was superheated, saturated, and subcooled, respectively. The results indicated that the heat transfer coefficient in superheat zone is significantly higher than correlations proposed for single-phase turbulent flow, and the condensation was identified from the tube wall temperature below saturation temperature. This superheat zone accounts for a significant portion of the heat rejected in the subcritical cycle and affects on condenser sizing.

Keywords:

CO_2, condensation, heat transfer, horizontal tube, critical point

Nomenclature

P	pressure	[Pa]
T	temperature	[^oC]
h	specific enthalpy	[J kg^{-1}]

x	vapor quality	[-]
q	heat flux	[W m^{-2}]
$\dot{Q}$	heat transfer rate	[W]
Z	tube length	[m]
m	mass flow rate	[kg s^{-1}]
G	mass flux	[kg $m^{-2}s^{-1}$]
d_i	inner diameter	[m]
d_o	outer diameter	[m]
h_{LV}	latent heat	[J kg^{-1}]
Cp	isobaric heat capacity	[J $kg^{-1}K^{-1}$]
$\overline{Cp}$	mean isobaric heat capacity = (h_{wi} - h_b) / (T_{wi} - T_{rb})	[J $kg^{-1}K^{-1}$]
f	friction factor	[-]
Re_{LO}	liquid only Reynolds number = $G_r\, d_i / \mu_L$	[-]
Re_L	superficial liquid Reynolds number = $G_r (1 - x)\, d_i / \mu_L$	[-]
Nu	Nusselt number	[-]
Pr	Prandtl number	[-]
Fr	Froude number	[-]
We	Weber number	[-]
Ga	Galileo number	[-]
g	gravitational acceleration	[$m\ s^{-2}$]

Greek symbols

α	heat transfer coefficient	[W $m^{-2}K^{-1}$]
ξ	void fraction	[-]
ρ	density	[kg m^{-3}]
μ	viscosity	[Pa·s]
λ	thermal conductivity	[W $m^{-1}K^{-1}$]

Subscripts

r	refrigerant
H2O	water
wi	interior tube wall or evaluated at interior tube wall temperature
b	evaluated at bulk temperature
f	evaluated at film temperature
sat	saturation temperature
V	vapor (evaluated at saturation temperature in two-phase zone)
L	liquid(evaluated at saturation temperature in two-phase zone)
TSi	test section inlet
TSo	test section outlet
PCi	pre-cooler inlet
PCo	pre-cooler outlet
MC	mixer

$_{M}$	momentum change term
$_{F}$	friction term
$_{gain}$	heat leak from ambient air
$_{cond}$	conduction heat
$_{crit}$	critical point

1. Introduction

From autumn to spring, outdoor units of CO_2 commercial refrigeration systems and some other applications spend most operating hours in the subcritical cycle. Although the rating condition of the summer season takes a transcritical cycle, it is necessary to understand the characteristics of the subcritical cycle to ensure reliable system performance and to evaluate the annual performance. The superheat of the subcritical cycle is relatively higher than a conventional cycle running at low reduced pressure. Therefore, it is important to understand the characteristics of heat rejection from superheated vapor in order to determine the proper size or to design circuits of condensers (gas coolers). Despite the importance of this, very limited information about this heat rejection process has been reported. As a first step, this paper provides the results of experiments conducted on the CO_2 pressure drop of subcritical condensation.

Bell (1972) described a desuperheating in condenser entrance, where the condensation may occur on cold surface exposed to superheated vapor. The criterion of the condensation occurrence was assumed as the cooling surface temperature which is below saturation point. With this criterion, it is suggested that simple use of LMTD method to calculate the overall coefficient of condensers could be invalid.

Fujii et al. (1978) measured the heat transfer coefficient (HTC) of R11 and R113 condensation flow in horizontal smooth tubes, and Lee et al. (1991) measured the HTC of R22. Fujii et al. also measured the temperature distribution of vapor flow in the radial direction of a tube and proved that vapor is superheated even when the vapor mass quality is below 1.0. These studies manipulated sensible heat rejection from superheated vapor in the condensation process and provided semi-rational empirical prediction methods. Their method considering sensible heat of condensation heat transfer would be informative for the discussion of very beginning of condensation occurrence, where sensible heat rejection is still considerable.

Jiang et al. (2007) presented experimental results on HTC of R404 A and R410 A in horizontal smooth copper tubes with inner diameters of 9.4 and 6.2 mm at reduced pressures of 0.8 and 0.9. They concluded that the effect of pressure was not significant in their experimental conditions, and the correlation proposed for lower reduced pressure by Cavallini et al. (2006) predicts condensation heat transfer well.

Koyama et al. (2008) presented experimental results and modified correlation for HTC, void fraction, and pressure drop of CO_2 condensation flow in a horizontal micro-fin copper tube 5.67 mm of equivalent inner diameter at 5 and 6 MPa. They concluded that the pressure drop and HTC decreased with rising pressure due to dense vapor and decreasing latent heat.

Hrnjak et al. (2002, 2008, 2009a) carried out some experiments focusing on condensation of CO_2 at low temperatures of -15 and -25^{o}C, where the low stage of cascade systems operates. Their findings confirmed the applicability of Cavallini's correlation in these conditions because of the similarity in thermophysical properties of R22 at high heat rejection temperatures (35^{o}C) and R744 at low temperatures (-15 to -30^{o}C).

However, data on HTC and pressure drop of the superheat zone have not been reported in any publication known to the authors.

2. Experimental set-up and methodology

Figure 1 shows a schematic diagram of the experimental apparatus which consists of circuits for CO_2, water, and chilled water of about 7°C. The components of the CO_2 circuit include a variable speed gear pump, a coriolis-type mass flow meter, an electric pre-heater, a mixer, a pre-cooler which is an counter-flow double-tube type heat exchanger, a test section which is a test tube surrounded by a thick brass jacket, two after-coolers, and a receiver tank. In the mixer placed at the entrance of the pre-cooler, the bulk-mean temperature and pressure of the superheated vapor are measured. Subcooled refrigerant kept in the receiver tank to maintain the proper refrigerant flow rate is controlled by the rate of chilled water flowing through the after-coolers. Cycle pressure is roughly controlled by the amount of CO_2 charge and precisely controlled by the after-coolers.

The measurement procedure for a two-phase zone, specifically, when superheat is below 5 K, is as follows. The superheat of refrigerant flowing through the mixer is kept at 3 to 5 K by the pre-heater for determining the bulk enthalpy; meanwhile, the inlet condition of the test section is controlled by the flow rate and inlet temperature of cooling water flowing through the pre-cooler. The measurement procedure for a superheat zone, specifically, when superheat is above 5 K, is as follows. The superheat of the test section inlet within 5 to 25 K is controlled by excitation of the pre-heater. While, the water flow of the pre-cooler is shut off.

2.1 Test section

Figure 2 (a) and (b) show the dimensions of the test section. The test tube, which is a smooth copper tube with an inner diameter of 6.1 mm and outer diameter of 9.53 mm, is placed horizontally and covered with a thick brass jacket. The gap between the tube and the jacket is filled with a thermal paste. On the outside of the brass jacket, copper tubes are attached with solder allowing cooling water to flow through. This structure yields cooling conditions with an almost uniform temperature. Twelve thermocouples are embedded into the top, bottom, right, and left of the test tube wall at three positions in an axial direction. Outside the bass jacket, two holes of 1 mm diameter are bored through the test tube wall as pressure ports and connected to the differential pressure transducer with capillary tubes. This pressure port structure makes it possible to measure pressure drop without any connectors changing inner diameter. The active cooling length by the brass jacket is 150 mm, and the length between pressure ports is 288 mm.

2.2 Data reduction method

Figure 3 shows an overview of the data reduction method. The main measured values are the refrigerant mass flow rate m_{r}, bulk-mean temperature $T_{\mathrm{rb,MC}}$, and absolute pressure P_{MC} in the mixer, the bulk water temperature of pre-cooler inlet $T_{\mathrm{H2O,PCi}}$ and outlet $T_{\mathrm{H2O,PCo}}$, test section inlet $T_{\mathrm{H2O,TSi}}$ and outlet $T_{\mathrm{H2O,TSo}}$, and the water mass flow rate of pre-cooler $m_{\mathrm{H2O,PCi}}$ and test section $m_{\mathrm{H2O,TSi}}$. The bulk-mean enthalpy in the mixer $h_{\mathrm{rb,MC}}$ is obtained from $T_{\mathrm{rb,MC}}$ and P_{MC} under the assumption of equilibrium by Refprop Ver 8.0. The enthalpy changes through the pre-cooler Δh_{PC} and the test section Δh_{TS} are determined by water side heat balances $\dot{Q}_{\mathrm{PC}}$ and $\dot{Q}_{\mathrm{TS}}$ as below.

$$\Delta h_{\mathrm{PC}} = \dot{Q}_{\mathrm{PC}} \Big/ m_{\mathrm{r}} = \left(\dot{Q}_{\mathrm{H2O,PC}} - \dot{Q}_{\mathrm{gain,PC}} \right) \Big/ m_{\mathrm{r}} \tag{1}$$

$$\dot{Q}_{\mathrm{H2O,PC}} = \left(T_{\mathrm{H2O,PCo}} - T_{\mathrm{H2O,PCi}}\right) m_{\mathrm{H2O,PC}} Cp_{\mathrm{H2O}} \tag{2}$$

$$\Delta h_{\mathrm{TS}} = \dot{Q}_{\mathrm{TS}} \Big/ m_{\mathrm{r}} = \left(\dot{Q}_{\mathrm{H2O,TS}} - \dot{Q}_{\mathrm{gain,TS}}\right) \Big/ m_{\mathrm{r}} \tag{3}$$

$$\dot{Q}_{\mathrm{H2O,TS}} = \left(T_{\mathrm{H2O,TSo}} - T_{\mathrm{H2O,TSi}}\right) m_{\mathrm{H2O,TS}} Cp_{\mathrm{H2O}} \tag{4}$$

where $\dot{Q}_{\mathrm{gain,PC}}$ and $\dot{Q}_{\mathrm{gain,TS}}$ are preliminarily measured heat leak from ambient air through the insulators. The averaged heat flux of the test section on the interior tube wall q_{wi} is,

$$q_{\mathrm{wi}} = \left(\dot{Q}_{\mathrm{H2O,TS}} - \dot{Q}_{\mathrm{gain,TS}} - \dot{Q}_{\mathrm{cond}}\right) \Big/ \left(d_{\mathrm{i}} \cdot \pi \cdot \Delta Z_{\alpha}\right) \tag{5}$$

where $\dot{Q}_{\mathrm{cond}}$ is the conduction heat from outside the cooling brass jacket as described in the Appendix A. The central refrigerant temperature (i.e. reference temperature of refrigerant) of test section T_{rb} is defined as an arithmetic mean of inlet and outlet bulk temperatures $T_{\mathrm{rb,i}}$ $T_{\mathrm{rb,o}}$, which are found from each pressure P_{TSi} and P_{TSo} and enthalpies $h_{\mathrm{b,i}}$ and $h_{\mathrm{b,o}}$ at equilibrium. With this method, the reference temperature of HTC T_{rb} smoothly changes from the bulk temperature to the saturation temperature at the vapor quality 1.0. The definition of averaged heat transfer coefficient α_{r} is,

$$\begin{aligned} &\alpha_{\mathrm{r}} = q_{\mathrm{wi}} \Big/ \left(T_{\mathrm{rb}} - T_{\mathrm{wi}}\right) = q_{\mathrm{wi}} \Big/ \left(\frac{T_{\mathrm{rb,i}} + T_{\mathrm{rb,o}}}{2} - T_{\mathrm{wi}}\right) \\ &T_{\mathrm{rb}} \approx T_{\mathrm{sat}} \quad at \quad 0 < x_{\mathrm{b}} < 1 \end{aligned} \tag{6}$$

where T_{wi} is the averaged temperature of the 12 points on the tube wall. The averaged pressure drop gradient is defined with the length between pressure ports ΔZ. The momentum term and friction term are described as,

$$\frac{\Delta P_{\mathrm{TS}}}{\Delta Z} = \left\{ \Delta P_{\mathrm{M}} + \left(\frac{dP_{\mathrm{F}}}{dZ}\right) \Delta Z \right\} \Big/ \Delta Z \tag{7}$$

Table 1 lists the test conditions of the test section. Table 2 lists the measurement uncertainties obtained from the results of two standards of calibration, resolution of data loggers and calibration equipment, and the

stability of excitation voltages. The maximum range of the differential pressure transducer is 0.75 kPa and the two standard deviations of calibration by atmosphere and nitrogen vapor was 17 Pa. However, the zero-point fluctuates when the transducer has some liquid CO_2 inside due to few millimeters of liquid head and capillary effect. The uncertainty 0.26 kPa listed in Table 2 is about the maximum of this fluctuation range.

3. Results and discussion

3.1 Categorization of heat rejection process

Figure 4 (a) and (b) show experimental results at 10 kW m^{-2} and 150 kg $m^{-2}s^{-1}$ at pressure 6 and 7 MPa respectively. In those figures, the horizontal axes show the bulk-mean enthalpy h_b and the top axes in upper graphs show vapor quality x_b. This vapor quality x_b is obtained as an equilibrium vapor quality from bulk-mean enthalpy and does not represent true vapor mass flow rate to total mass flow rate. Cavallini et al. (2006) call this "thermodynamic vapor quality" in their paper. The upper graphs show the bulk-mean refrigerant temperature of the test section inlet $T_{rb,i}$ and outlet $T_{rb,o}$, averaged tube wall temperatures T_{wi}, and averaged heat flux q_{wi}. The center graphs show the averaged HTC α_r of the test section and five comparative correlations. The bottom graphs show the pressure drop $\Delta P_{TS}/\Delta Z$ and comparative correlations. The bars show measurement uncertainties vertically and enthalpy changes through the test section horizontally.

As shown with $T_{rb,i}$ and $T_{rb,o}$ along with the flow directions, the refrigerant releases mostly its sensible heat first as a decrease in temperature, then releases latent heat at the saturation temperature. Following the conventional approach, the heat rejection process is specifically categorized as superheat, two-phase, and

subcool zone with bulk-mean enthalpy. The point of note is that this categorization is based on bulk-mean enthalpy or temperature, but not film or wall temperature. Correctly, the refrigerant starts releasing latent heat before enters the two-phase zone of above categorization. This start point of condensation is hereinafter discussed.

3.2 Comparison to correlations

Table 3 lists correlations for the HTC compared in Fig. 4. In the two-phase zone, the experimental HTC (circles) was compared to the correlation for condensation flow of other refrigerants in smooth tubes proposed by Cavallini (2006) and Haraguchi (1994). These correlations were developed on experimental data obtained at much lower reduced pressures. Cavallini's correlation showed the best agreement to the experimental HTC in several reports, as Jiang et al. (2007) concluded in their paper focusing on condensation of R410A at reduced pressure 0.8 and 0.9 and experimental results support that conclusion. In the superheat zone, the correlations proposed for single-phase turbulent flow in smooth circular pipes by Dittus-Boelter (1930), Petukhov (1970), and Gnielinski (1975) are plotted. At high superheat, the experimental HTC is well predicted by those correlations, while when latent heat is exchanged prediction is poor.

Table 4 lists comparative correlations for the pressure drop in Fig. 4. In the two-phase zone, Friedel's correlation (1979) agrees with the experimental pressure drop satisfactorily at lower pressure 6MPa. In the superheat zone, Colburn's correlation (1933) is compared to the experimental pressure drop. The experimental pressure drop is slightly higher than the correlation in that zone.

3.3 Identification of condensation in superheat zone

Figure 5 shows the changes in refrigerant properties in the superheat zone to support discussion of the deviation of the experimental HTC from the correlations proposed for single-phase turbulent flow, as mentioned above. The density increases about twofold at 7 MPa from 470 kJ kg^{-1} to 380 kJ kg^{-1}, which is almost the saturation point. This means the vapor velocity decreases by about half, but the HTC of forced convection increases because the Prandtl number increases about seven times. However, the effects of change in thermophysical properties are calculated by the correlations and do not explain why the experimental HTC starts increasing from the predicted values as the tube wall temperature reaches saturation temperature.

Figure 6 illustrates the temperature profile measured by Fujii et al (1978). The temperature profile of the core vapor flow shown in the top illustration, which is measured on the middle horizontal plane of a horizontal smooth tube, shows that the core vapor flow is superheated even under the condensing condition. The deviation of HTC from the correlations of single-phase turbulent flow in superheat zone can be explained with this radial temperature distribution as following.

Figure 7 shows the estimated radial profile of the temperature and Prandtl number of superheated vapor at 7 MPa and 150 kg $m^{-2}s^{-1}$. Based on the measurement results of Fujii et al., the temperature profile is close to von Karman's universal profile of turbulent flow. The radial profile is estimated from the measured bulk-mean refrigerant and tube wall temperature, with a supplementary line between them from the universal temperature profile at $Z/d_i = 20$ measured by Hishida et al. (1977). Figure 7 (a) is the profile at 400 kJ kg^{-1}, in which the tube wall temperature is below 3.1 K from the saturation. Figure 7 (b) is at 422 kJ kg^{-1}, a condition in which the tube wall temperature barely reached the saturation temperature. The main core vapor flow is superheated; however, the tube wall temperature has some subcooling, that is, 3.1 and 0.8 K, which indicates condensation. Additionally, the condensation is corroborated by more evident deviation at 6 MPa than 7 MPa,

as shown in Fig. 4, because the ratio of latent heat to sensible heat in total rejected heat is much higher at 6 MPa than at 7 MPa. Also, the fact that the experimental HTC merges with Cavallini's correlation that predicts condensation HTC at $x_b = 1.0$ supports this.

3.4 Effects of mass flux, heat flux, and pressure on HTC

Figures 8 (a) and (b) show the experimental HTC for various mass and heat fluxes, compared to correlations by Cavallini for the two-phase zone and Gnielinski for the superheat and subcool zones. As shown in the right graph of Fig. 8 (a), HTC increases with increasing mass flux in the two-phase zone. Cavallini's correlation shows very good fidelity at 6 MPa. When approaching critical pressure (7 MPa), correlation does not predict as good as lower pressure 6 MPa but shows expected relation with increasing mass flux. The reason is described in Sub Section 3.5.

As shown in Fig. 8 (b), in the superheat zone, Gnielinski's correlation deviates more at higher heat fluxes and closer to saturation. This is because higher heat flux causes the tube wall temperature to decrease and reach the saturation temperature earlier, which means that high heat flux causes the superheated vapor to start condensing earlier. In the two-phase zone, the experimental HTC increases with the increasing heat flux and the incremental plateaus at 15 kW m^{-2}. On the other hand, the correlation shows that HTC decreases same as Nusselt's film-wise condensation theory (1916). According to that theory, the growing liquid film due to higher heat flux acts as a heat resistance and decreases HTC. However, this theory proposed for laminar-free convection condensation assumes quiescent vapor and ignores the forced convection by flowing superheated vapor. The experimental HTC in the right graph of Fig. 8 indicates limited increase with increasing heat flux.

Figure 9 shows the transition of HTC through the component of refrigeration cycles, condenser. This

figure shows HTC along four isobars (5, 6, 7 and 7.5 MPa) as a function of the bulk mean enthalpy h_b at 100 kg $m^{-2}s^{-1}$ and 10 kW m^{-2}. Those four graphs on HTC are inserted in the p-h diagram. The experimental HTC (circular symbols) lay on the top of correlations (lines) in the range for which they are developed. Below the critical pressure, the deviation of the experimental HTC from the correlation is shown approximately from enthalpy 450 kJ kg^{-1} to the saturation curve. This is the zone where condensation occurs in the presence of superheated vapor. The HTC just above the critical pressure at 7.5 MPa is discussed in Section 3.6.

3.5 Heat rejection and pressure drop around the critical point

Figure 10 shows the experimental results (circular symbols) and correlations (lines) of HTC and the pressure drop at an enthalpy of 320 to 360 kJ kg^{-1}. The horizontal axis shows pressure. As apparent in Fig. 10 (a), the experimental HTC decreases monotonically with rising pressure until 7.3 MPa. While, Cavallini's correlation predicts earlier change at 6.5 MPa. The pressure 6.5 MPa, reduced pressure P/P_{crit} = 0.88, is much higher than the validity range of Cavallini's correlation. For improving the correlations of heat transfer above reduced pressure 0.88, the following elements should be taken into account:

- Thicker liquid film due to lower liquid density.
- Low vapor velocity due to higher vapor density.
- Temperature distribution in liquid film caused by higher specific heat of liquid.
- Significantly increasing Prandtl number of liquid and vapor towards the critical pressure.
- Significantly increasing sensible heat rejection and decreasing latent heat rejection
- Waves on the liquid surface due to lower surface tension.

As shown in Fig. 10 (a), the experimental HTC starts increasing at 7.3 MPa and then decreases again at 7.5 MPa. As shown in Fig 10 (b), the experimental pressure drop decreases and then suddenly rises steeply at 7.2 MPa, then drops again at the critical pressure, which is approximately 7.4 MPa. Likewise, those transitions occur at slightly different pressures. These results in Fig. 10 (a) and (b) have some similarities to the findings obtained in previous research on film-wise condensation on a vertical cold wall.

Fujii and Watabe (1987) derived the Nusselt number of laminar condensation on vertical cooling plate with the stream functions from the governing equations and also confirmed it experimentally with subcritical CO_2 and water vapor. Their main conclusions are follows. Nusselt's theory is able to be extended to very near the critical point with the fluid properties at the film temperature. HTC constantly decreases until 7.3 MPa and then starts increasing toward the critical point. Although the experimental results are indistinct, HTC shows a turning point at about 7.3 MPa, and this agrees with their conclusions. However, the reason HTC peaked at 7.5 MPa (just above the critical pressure) is still unknown. On the other hand, Ishihara et al. (2002) observed the behavior of falling liquid of subcritical CO_2. According to their visualization, the behavior changes to a random steeple-shaped wave from a laminar or periodic waves at 7.2 MPa due to decreasing surface tension. Also, the experimental pressure drop had an obvious turning point at 7.2 MPa, which might be explained by the momentum dissipation at the complex liquid surface.

3.6 Modification for subcritical two-phase zone HTC based on Cavallini's correlation

As stated above, the temperature distribution in the condensed liquid film is not negligible near the critical point primarily due to higher specific heat. Therefore the liquid properties should be evaluated at the film temperature. As a trial, Cavallini's correlation (2006) is modified using the approach of Fujii and Watabe

(1987). The summary of this modified correlation is as below.

$$
\left.
\begin{aligned}
&J_G = xG_{\mathrm{r}} \Big/ \sqrt{gd_{\mathrm{i}}\rho_{\mathrm{V}}\left(\rho_{\mathrm{L}}-\rho_{\mathrm{V}}\right)}\,,\; J_G{}^T = \left\{\left(7.5/4.3X_{tt}{}^{1.111}+1\right)^{-3}+2.6^{-3}\right\}^{-1/3} \\
&\alpha_{\mathrm{LO\_f}} = 0.023\left(G_{\mathrm{r}}d_{\mathrm{i}}/\mu_{\mathrm{L\_f}}\right)^{0.8} Pr_{\mathrm{L\_f}}{}^{0.4}\left(\lambda_{\mathrm{L}}/d_{\mathrm{i}}\right) \\
&\alpha_{\mathrm{strat}} = 0.725\left\{1+0.741\left(\frac{1-x}{x}\right)^{0.3321}\right\}^{-1}\left[\frac{\lambda_{\mathrm{L\_f}}{}^3\rho_{\mathrm{L\_f}}\left(\rho_{\mathrm{L\_f}}-\rho_{\mathrm{V}}\right)gh_{\mathrm{LV}}}{\mu_{\mathrm{L\_f}}d_{\mathrm{i}}(T_{\mathrm{wi}}-T_{\mathrm{sat}})}\right]^{0.25} + \left(1-x^{0.087}\right)a_{\mathrm{LO\_f}} \\
&\alpha_{\mathrm{r}} = \begin{cases} J_G > J_G{}^T : \alpha_{\mathrm{A}} = \alpha_{\mathrm{LO\_f}}\left[1+1.128x^{0.8170}\left(\rho_{\mathrm{L}}/\rho_{\mathrm{V}}\right)^{0.3685}\left(\mu_{\mathrm{L}}/\mu_{\mathrm{V}}\right)^{0.2363}\left(1-\mu_{\mathrm{V}}/\mu_{\mathrm{L}}\right)^{2.144}Pr_{\mathrm{L\_f}}{}^{-0.1}\right] \\ J_G \le J_G{}^T : \left[\alpha_{\mathrm{A}}\left(J_G{}^T/J_G\right)^{0.8}-\alpha_{\mathrm{strat}}\right]\left(J_G/J_G{}^T\right)+\alpha_{\mathrm{strat}} \end{cases}
\end{aligned}
\right\} \quad (8)
$$

where the subscription "_f" is the liquid properties evaluated at the film temperature (T_{sat} + T_{wi}) / 2. Cavallini's correlation is composed of forced convection heat transfer term based on Dittus-Boelter correlation (1930) and free convection of falling film heat transfer term based on Nusselt's correlation (1916). In those terms, the relevant liquid properties are evaluated at the film temperature. However, other properties relevant to the parameters predicting the effect of flow regime J_G and $J_G{}^T$, which Cavallini et al. found from huge data base, are not changed except liquid Prandtl number.

Figure 10 (a) also shows the calculation results of above modified correlation Eq. (8). The original correlation of Cavallini et al. deviates above 6.5 MPa. On the contrary, the modified correlation agrees well with the experimental results not only in subcritical region but also at lower pressure below 6.5 MPa. Despite of very simple modification, this allows Cavallini's correlation to accurately predict HTC until reduced pressure 0.97.

3.7 Similarity between supercritical gas cooling and superheat zone condensation

As shown in Fig. 9, about 7.5 MPa, just above the critical pressure, Gnielinski's correlation shows extremely high HTC due to the thermal properties. For comparison, the figure also shows dashed-dotted and dashed

lines that represent Petrov and Popov's (1985) and Dang and Hihara's (2007) proposed methods to predict transcritical gas cooling. Their methods take into consideration the strong fluid property distribution in the tube radius near the pseudo-critical temperature. Hence the maximum HTC of Petrov and Popov's and Dang and Hihara's correlations are much closer to the experimental HTC.

Although the liquid surface vanishes, liquid and gas (not to be called vapor) phases still occur above the critical pressure in the molecular dynamic study. At the very least, the properties change drastically during the small temperature difference around the pseudo-critical temperature, which is similar to a phase change from vapor to liquid. Thus, a similar phenomenon to superheat zone condensation occurs in the supercritical heat rejection process when the pseudo-critical temperature is sandwiched between the bulk and wall temperatures. For instance, if the experimental HTC is 2.5 kW m^{-2} K^{-1} and the bulk refrigerant temperature is 31.8 ^{o}C around the pseudo-critical point of 350 kJ kg^{-1}. Hence, the temperature difference is 4 K, the tube wall temperature is 27.8^{o}C, and the refrigerant enthalpy at 27^{o}C is 278 kJ kg^{-1}. This means the enthalpy is radially distributed from 350 to 278 kJ kg^{-1}. This large enthalpy change is comparable to latent heat, and the HTC should be determined by the thermal properties of this averaged value. Consequently, the lower maximum HTC shown in the experimental results and in Petrov and Popov's and Dang and Hihara's correlations are rational.

Furthermore, the supercritical HTC has the maximum point above the pseudo-critical temperature for the similar reason of superheat zone condensation. The refrigerant flow facing the tube wall reaches a pseudo-critical point ahead of the core flow. Likewise, it was confirmed theoretically and experimentally by Goldman (1961), Tanaka et al. (1968) and Yamagata et al. (1972) that the maximum HTC appears just above the pseudo-critical temperature under cooling conditions and just below it under heating conditions.

3.8 Effect of condensation in superheat zone on sizing of air cooled heat exchangers

As shown in Fig. 9, condensation in the superheat zone causes deviation from correlations but could be more important at higher reduced pressure due to greater portion of enthalpy change in that zone relative to two-phase zone. In addition, a higher compressor discharge temperature increases the importance of the condensation in the superheat zone in selecting the size of the heat exchanger. Both higher HTC and greater temperature difference between refrigerant and air can potentially reduce the size of condensers.

Figure 11 shows an example of rough calculation on heat flux when a cross-finned tube type condenser is used. There is some concern that the heat resistance on the air side might reduce the beneficial effects of heat transfer of the refrigerant side. The air side HTC, surface area enlargement, fin efficiency, and contact heat resistance are assumed as shown in the left graph of Fig. 11. The heat conduction through the fins caused by the refrigerant temperature gradient is ignored. Furthermore, the inlet air temperature is assumed uniformly below 5 K of refrigerant saturation temperature at 7 MPa, which is a typical condition in spring and autumn. The refrigerant side HTC is assumed to have the value shown by the solid curve in the upper right graph in Fig. 11 which is based on the experimental results at 6 MPa, 100 kg $m^{-2}s^{-1}$ and 10 kW m^{-2}. The solid curve considering superheat zone condensation is compared to the Gnielinski's correlation shown with dashed curve. The calculation results are shown in the bottom right graph in Fig. 11. The heat flux on the interior tube wall taking superheat zone condensation into account is shown with a solid line; if ignoring superheat zone condensation, it is shown with a dashed line. The difference indicates the potential to reduce the size of the heat exchanger, nevertheless the large heat resistance of air side.

4. Conclusions

This paper has presented the experimental results of heat rejection transfer and pressure drop under uniform temperature cooling in a horizontal smooth tube around the critical point of CO_2. These results include condensation in a two-phase zone and a superheat zone, in addition to supercritical gas cooling.

In the superheat zone, the HTC is well predicted by correlations proposed for single-phase turbulent in-tube flows at the high superheat. However, the experimental HTC starts to increase from the correlations when the tube wall reaches saturation temperature and gradually merges into Cavallini's correlations at the vapor quality of 1.0. The deviation from the single-phase correlations is more evident at 5 and 6 MPa than at 7 MPa. These clearly identify the occurrence of condensation in the superheat zone.

In the two-phase zone, the experimental HTC are predicted well with Cavallini's correlation up to 6 MPa. The correlation deviated slightly at 7.0 MPa. The experimental HTC at 344 kJ kg^{-1} increases as the mass flux and heat flux increases. The HTC decreased with rising pressure up to 7.3 MPa, then increased until 7.5 MPa, and then decreased again. On the other hand, the experimental pressure drop at 344 kJ kg^{-1} decreased with rising pressure until 7 MPa and suddenly rose sharply at 7.2 MPa, then dropped down at the critical pressure. These tendencies have some similarities with previous studies of film-wise condensation on vertical cooling plates.

Just above the critical pressure at 7.5 MPa, the experimental HTC reached a maximum a bit above the pseudo-critical point of bulk enthalpy, and the maximum value was much lower than Gnielinski's correlation because of strong changes of properties in the tube radius. A correlation by Petrov and Popov, and Dang and Hihara accounting for the radial property changes was much closer to the experimental HTC than the

Gnielinski correlation for this condition

Acknowledgements

We gratefully acknowledge the financial support from the Air Conditioning and Refrigeration Center (ACRC) at the University of Illinois and the technical support (access to instrumentation and their facility) from Creative Thermal Solutions (CTS).

Appendices

A. Conduction heat from out of the test section through the test tube

The refrigerant is cooled by water flowing through a thick brass jacket, and the heat-transfer-area is defined by the length of the jacket. However, the test tube conducts heat from out of the brass jacket, and the cooling water absorbs the heat. Since the length of the test section is short, it is necessary to confirm the effect of the heat conductivity. Figure A.1 shows the heat balance in one element of the length ΔZ. The italic subscripts $_{i}$, $_{j}$, $_{k}$ indicate the position of each element, and the heat balance in one element is represented as,

$$\begin{aligned} &\Delta\dot{Q}_{\text{tube,o}} = \Delta\dot{Q}_{\text{tube,in}} + \Delta\dot{Q}_{\text{r}} \\ &\begin{cases} \Delta\dot{Q}_{\text{tube,i}} = \lambda_{\text{tube}} \left\{ (d_{\text{o}} - d_{\text{i}})^2 \, \pi/4 \right\} \left(T_{\text{w},k} - T_{\text{w},j} \right) \\ \Delta\dot{Q}_{\text{tube,o}} = \lambda_{\text{tube}} \left\{ (d_{\text{o}} - d_{\text{i}})^2 \, \pi/4 \right\} \left(T_{\text{w},j} - T_{\text{w},i} \right) \\ \Delta\dot{Q}_{\text{r}} = \alpha_{\text{r}} \left(T_{\text{r},j} - T_{\text{w},j} \right) \left(d_{\text{i}} \pi \Delta Z \right) \end{cases} \end{aligned} \tag{A.1}$$

$$\therefore T_{\text{w},k} = 2T_{\text{w},j} - T_{\text{w},i} + \frac{\alpha_{\text{r}} \left(d_{\text{i}} \pi \Delta Z \right)}{\lambda_{\text{tube}} \left\{ (d_{\text{o}} - d_{\text{i}})^2 \, \pi/4 \right\}} \left(T_{\text{w},j} - T_{\text{r},j} \right) \tag{A. 2}$$

For simple calculation, the heat transfer coefficient α_r is assumed to be the same as the averaged value through the test section. Meanwhile, the refrigerant temperature $T_{r,j}$ is obtained with enthalpy change Δh as below,

$$h_j = h_k - \Delta h = h_k - \Delta \dot{Q}_r \Big/ \left\{ G_r (d_o - d_i)^2 \pi / 4 \right\} \tag{A. 3}$$

As the boundary condition, temperature $T_{w,root}$ at the root of the test tube is given as,

$$T_{w,root} = T_{r,root} - q_{wi} / \alpha_r \tag{A.4}$$

Figure A.2 shows the calculation results of heat conduction through a test tube with an inner diameter of 6.1 mm and outer diameter of 9.53mm. The horizontal axis is the HTC of the test section, the vertical axis is the heat conducted out of the test section, and the symbols are calculation results of the various conditions. The curves are empirical correlations as shown in Eq. (A.5). The heat conduction does not change with pressure and mass flux; however it increases with increasing heat flux and decreasing HTC. For data reduction, such heat conduction of the upstream and downstream is taken into account.

$$\dot{Q}_{cond} = \Delta \dot{Q}_{tube,o,root} = C_1 \ln(\alpha_r / 1000) + C_2 \quad [W]$$
$$\begin{cases} C_1 = -0.021 \left(q_{wi} / 1000 \right) - 0.0009 \\ C_2 = 0.057 \left(q_{wi} / 1000 \right) + 0.0022 \end{cases} \tag{A.5}$$

B. Effect of the thermal entry length

In the measurement of superheat above 5 K, the cooling water flow of the pre-cooler was shut off. Thus, refrigerant flow is thermodynamically developing, and hydrodynamically fully developed in the test condition. Since the test section was relatively short, the effect of thermal entry length was confirmed as below. The averaged HTC in a smooth tube of length Z is experimentally proposed as,

$$\alpha/\alpha_{\infty} = 1 + C/\left(Z/d_{\mathrm{i}}\right) \quad \text{(B.1)}$$

Here, C is the coefficient determined by the entrance condition, and was 1.4 in this case.

Figure B.1 is the calculation result of the thermal entry length, and it shows that the test section of the length $Z / d_{\mathrm{i}} = 25$ gave a 6% higher HTC than the fully developed HTC when the water flow of the pre-cooler was shut off.

References

ASME Performance Test Codes, 1985. Supplement on Instrument and Apparatus, Part1, ASNSI / ASME PTC 19.1-1985.

Bell, K. J, 1972. Temperature profiles in condensers, Chem. Eng. Prog., **68**, No.7, 81-82.

Bell, K. J, Muller, A. C., 2001. The Wolverine data book II, Wolverine Tube, Inc., 163-164, http://www.wlv.com/products/databook/databook.pdf

Cavallini, A., Del Col, D., Doretti, L., Matkovic, M., Rossetto, L., Zilio, C., and Censi, G., 2006. Condensation in horizontal smooth tubes: a new heat transfer model for heat exchanger design, Heat Trans. Eng., 27 (8) 31-38.

Colburn, A.P., 1933. A method of correlating forced convection heat transfer data and comparison with fluid friction, Trans. AIChE, **29**, 174-210.

Dang, C., and Hihara, E., 2003. Cooling heat transfer of supercritical carbon dioxide: A new correlation for heat transfer coefficient and effect of lubricant oil, Trans. JSRAE, 120, (2) 175-183 (in Japanese).

Dittus, F. W., Boelter, L. M. K., 1930. University of California, Berkeley,CA, Publicaions in Engineering **2**,

443.

Filonenko, G. K., 1954. Hydraulic drag in pipes, Teploenergetika, **1** No. 4, 40-44 (in Russia).

Fujii, T., Honda, H., Nozu, S., and Nakarai, S., 1978. Condensation of superheated vapor inside a horizontal tube, Heat Transfer - Japanese Research, 4 (3), 1-48.

Fujii, T., and Watabe, M., 1987. Laminar film condensation in the subcritical region – Gravity controlled condensation, JSME Trans. (B), 53 (490), 1801-1806 (in Japanese).

Friedel, L., 1979. Improved friction pressure drop correlations for horizontal and vertical two phase pipe flow, Proc. European Two-Phase Flow Group Meeting, Ispra, Italy, Paper no. E2.

Gnielinski, V., 1976. New equation of heat and mass transfer in turbulent pipe and channel flow. Int. Chem. Eng., **16**, 359-367.

Goldman, K., 1961. Heat transfer to supercritical water at 5000 psi flowing at high mass flow rate through round tubes, ASME Int. Dev. in Heat Transfer, Part III, 561-568.

Haraguchi, H., Koyama, S., Fujii, T., 1994. Condensation of refrigerants HCFC 22, HCFC 134a and HCFC 123 in a horizontal smooth tube (2nd report; Proposals of empirical expressions for local heat transfer coefficient), JSME Trans. (B), 60 (574) 2117-2124 (in Japanese).

Hishida, M., Nagano, Y., and Tagwa, M., 1977. Temperature distribution in the turbulent boundary layer in a circular pipe, Trans. JSME, 43(375), 4237-4245 (in Japanese).

Hufschmidt, W., Burck, E. and Riebold, W., 1966. Die bestimmung örtlicher und mittlerer wärmeübergangszahlen in rohren bei hohen wärmestromdichten, Int. J. Heat Mass Transfer, Vol. 9 (6), 539-565.

Ishihara, I., Mori, H., and Matsumoto, R., 2002. Behavior of condensate of carbon dioxide in subcritical

region, JSME Trans. (B), 68 (671), 1878-1883 (in Japanese).

Jang, J., and Hrnjak, P. S., 2002. Condensation of carbon dioxide at low temperatures, Proc. International Institute of Refrigeration Conference on Natural Refrigerants, Guangchou, 64-74.

Jang, J., and Hrnjak, P. S., 2003a. Flow regimes and heat transfer in condensation of carbon dioxide at low temperatures, Proc. HEFAT 2003, Victoria Falls.

Jang, J., and Hrnjak, P. S., 2004. Condensation of CO_2 at low temperatures, ACRC Report CR-56, June 2004.

Jiang, Y., Mitra, B., Garimella, S., and Andresen, C., 2007. Measurement of condensation heat transfer coefficients at near-critical pressures in refrigerant blends, Trans. ASME J. Heat transfer, 129, 958-965.

Kim, Y. J., Jang, J., Hrnjak, P. S., and Kim, M. S., 2008. Adiabatic horizontal and vertical pressure drop of carbon dioxide inside smooth and microfin tubes at low temperatures, J. Heat Transfer, 130:11.

Kim, Y. J., Jang, J., Hrnjak, P. S., and Kim, M. S., 2009a. Condensation heat transfer of carbon dioxide inside horizontal and vertical pressure smooth and microfin tubes at low temperatures, J. Heat Transfer, 131:2.

Kondou, C., Hrnjak, P. S., 2010. Heat rejection from R744 near the critical point, 13th Int. Refrig. A/C Conf. at Purdue, paper no. 2424.

Kondou, C., Hrnjak, P., 2010. Excellent Heat rejection from CO_2 near the critical point – opportunity for high efficiency, Sustainable Refrigeration and Heat Pump Technology, Stockholm, June 13-16, 2010.

Koyama, S., Kondou, C., and Kuwahara, K., 2008. An experimental study on condensation of CO_2 in a horizontal micro-fin tube, 12th Int. Refrig. A/C Conf. at Purdue, paper no. 2322.

Lee, C. C., Teng, Y. J., and Lu, D. C., 1991. Investigation of condensation heat transfer of superheated R-22 vapor in a horizontal tube, Proc. World Conf. Exp. Heat Trans. Fluid Mech. and Thermodynamics., 1051-1057.

Lemmon, E. W., Huber, M. L., and McLinden, M. O., 2007. Reference fluid thermodynamic and transport properties-REFPROP ver.8.0, National Institute of Standards and Technology, Boulder, CO, USA.

McAdams, W. H., 1954. Heat Transmission, 3rd ed., McGraw Hill, New York, 218-229.

Moffat, R. J., 1988. Description uncertainties in experimental results. Exp. Therm. Fluid Sci., 1, 3-17.

Nusselt, W., 1916. Die Oberflachenkondensation des wasserdampfes, Vereines Deutscher Ingenieure, Vol. 60, no. 27, p.541-546.

Park, C. Y., and Hrnjak, P. S., 2009b. CO_2 condensation heat transfer and pressure drop in multi-port microchannels, 3rd IIR Conference on Thermophysical Properties and Transfer Processes of Refrigerants, Boulder, CO, June 23-26, 2009.

Petrov, N. E., and Popov, V. N., 1985. Heat transfer and resistance of carbon dioxide being cooled in the supercritical region, Thermal Eng., **32** (3), 131-134.

Petukhov, B. S., 1970. Heat transfer and friction in turbulent pipe flow with variable physical properties, Advances Heat Transf., Academic Press, Orland, 6, 503-564.

Sieder, E. N. and Tate, G. E., 1936. Heat transfer and pressure drop of liquids in tubes, Ind. Eng. Chem. **28**.1429-1435.

Sleicher, C. A., and Rouse, M.W., 1975. A convenient correlation for heat transfer to constant and variable property fluid in turbulent pipe flow, Int. J. Heat Mass Transfer, **18**, 677-683.

Tanaka, H., Nishikawa, N., and Hirata, M., 1968. Turbulent heat transfer to supercritical carbon dioxide, Proc. 1967 Semi-International symposium Heat and Mass Transfer, Vol.2 127-134.

Yamagata, K., Nishikawa, K., Hasegawa, S., Fujii, T., and Yoshida, S., 1972. Forced convective heat transfer to supercritical water flowing in tubes, Int. J. Heat Mass Transfer, 15, 2575-2593.

Zilly, J., J. Jang, and Hrnjak, P. S., 2003c. Condensation of CO_2 at low temperature inside horizontal microfinned Tubes, ACRC Report No. CR-49, Mar. 2003.

Zilly, J., Jang, J., and Hrnjak, P. S., 2003b. Condensation of carbon dioxide at low temperatures in micro-finned horizontal tubes, Proc. International Institute of Refrigeration, Washington D.C.

Figure caption list

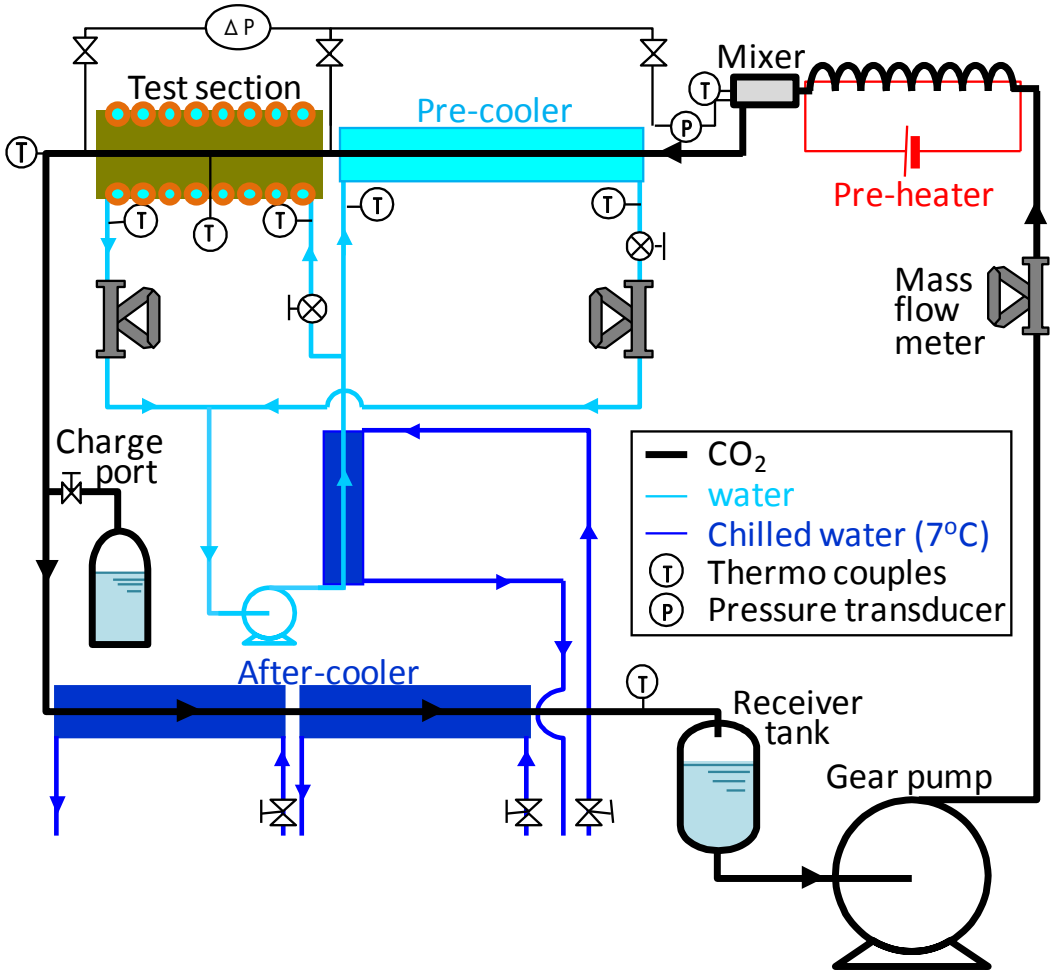

Figure 1 Schematic diagram of experimental apparatus

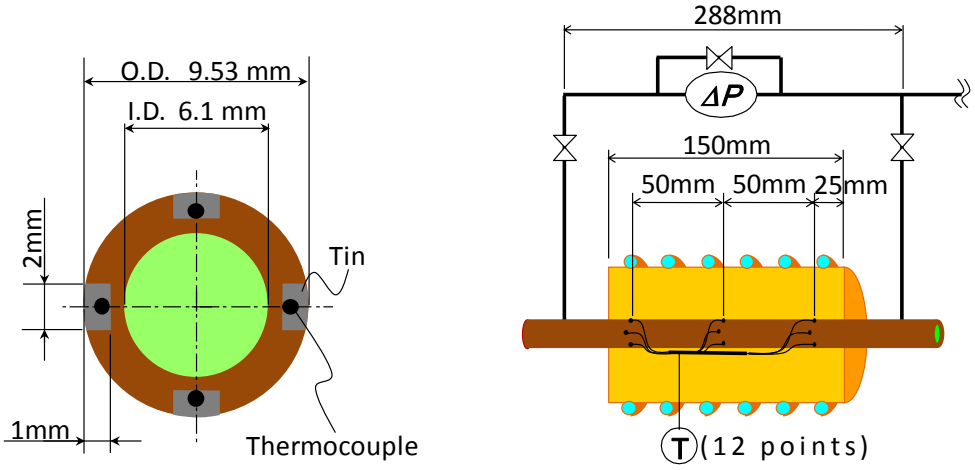

(a) Cross section of the test tube (b) Length of the test section

Figure 2 Dimensions of test section and positions of thermocouple

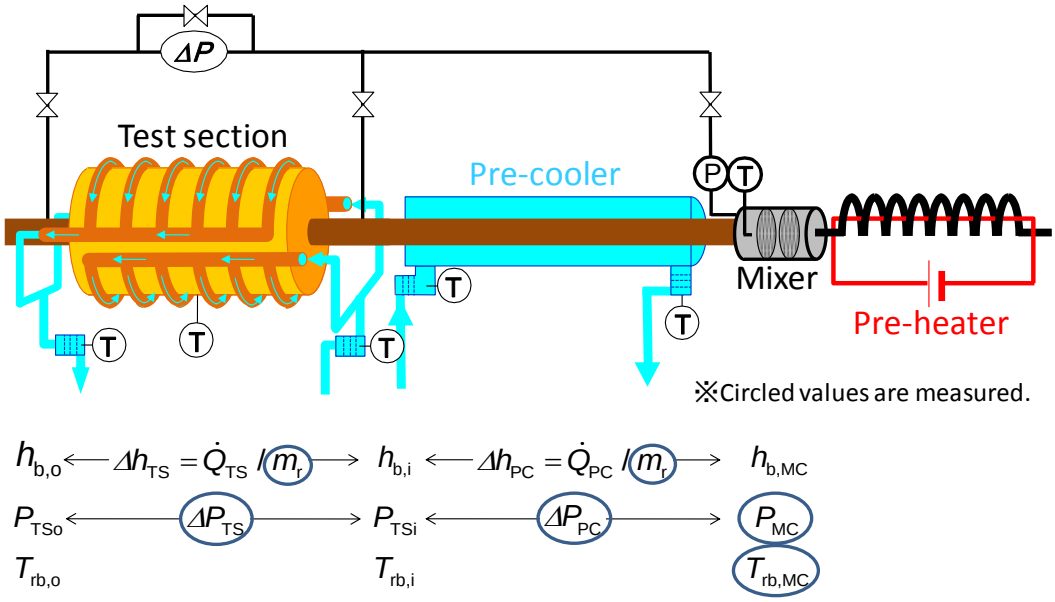

Figure 3 Overview of data reduction procedure

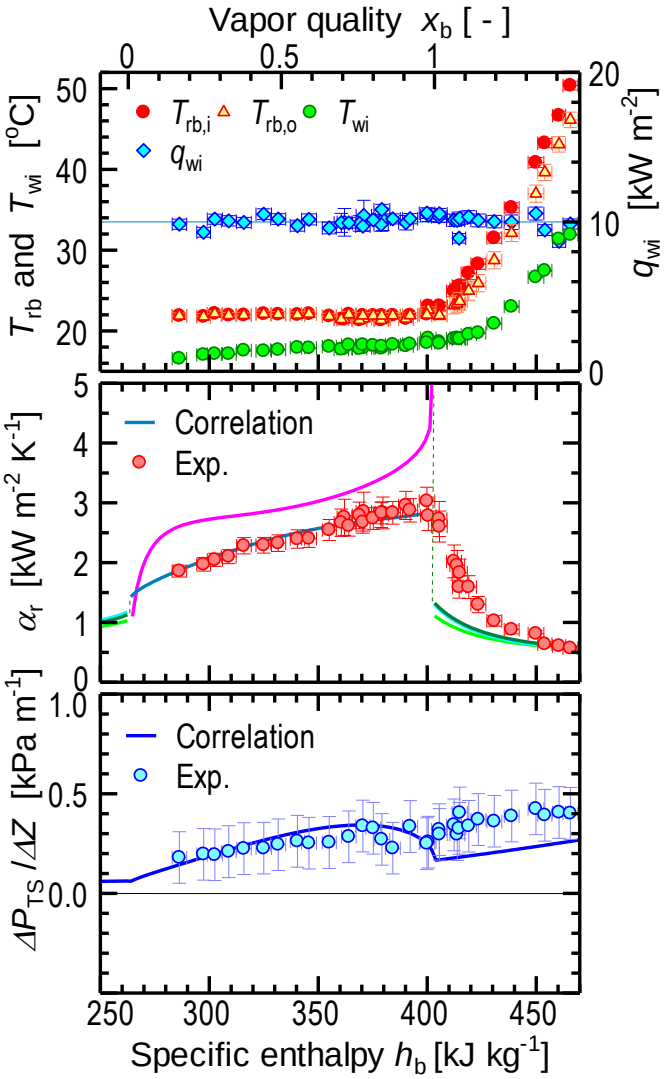
Vapor quality x_b [-]
0
0.5
1
$T_{rb,i}$
$T_{rb,o}$
T_{wi}
q_{wi}
T_{rb} and T_{wi} [°C]
q_{wi} [kW m^{-2}]
50
40
30
20
20
10
0
Correlation
Exp.
α_r [kW m^{-2} K^{-1}]
5
4
3
2
1
0
Correlation
Exp.
$\Delta P_{TS}/\Delta Z$ [kPa m^{-1}]
1.0
0.5
0.0
250
300
350
400
450
Specific enthalpy h_b [kJ kg^{-1}]

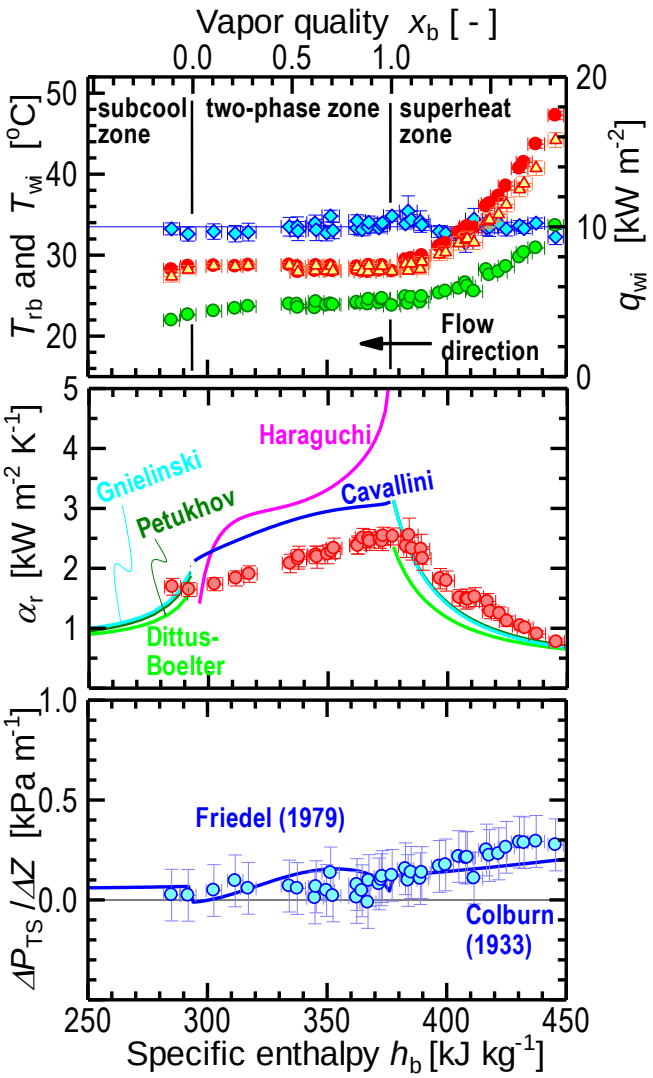

(a) 6.0 MPa, 10 kW m^{-2}, 150 kg m^{-2}s^{-1} **(b) 7.0 MPa, 10 kW m^{-2}, 150 kg m^{-2}s^{-1}**

Figure 4 Examples of detailed experimental results

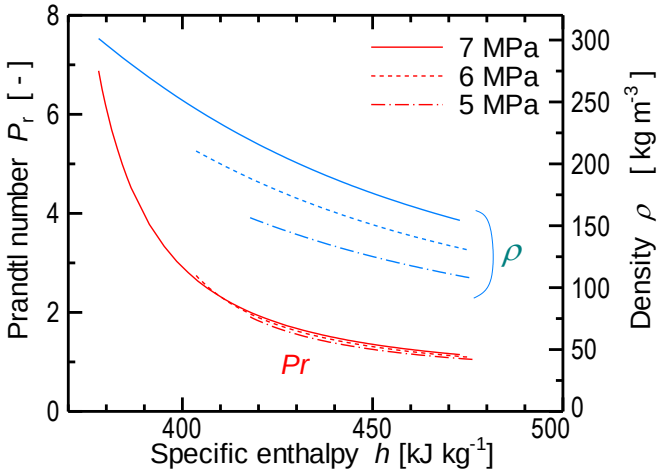

Figure 5 Changes in superheated vapor properties

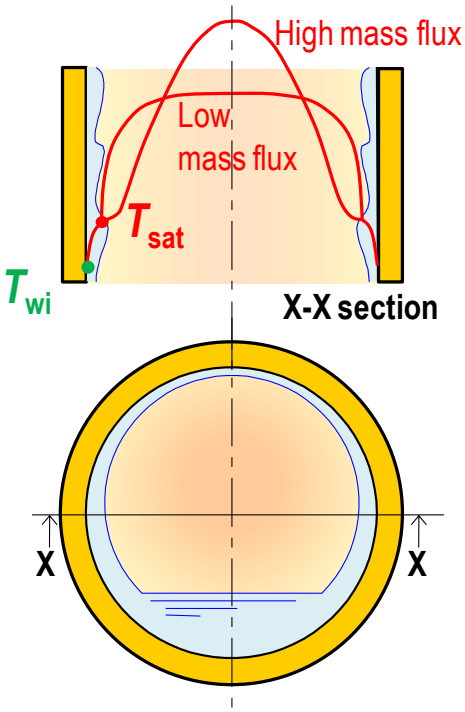

Figure 6 Illustration of radial temperature distribution measured by Fujii et al. (1978)

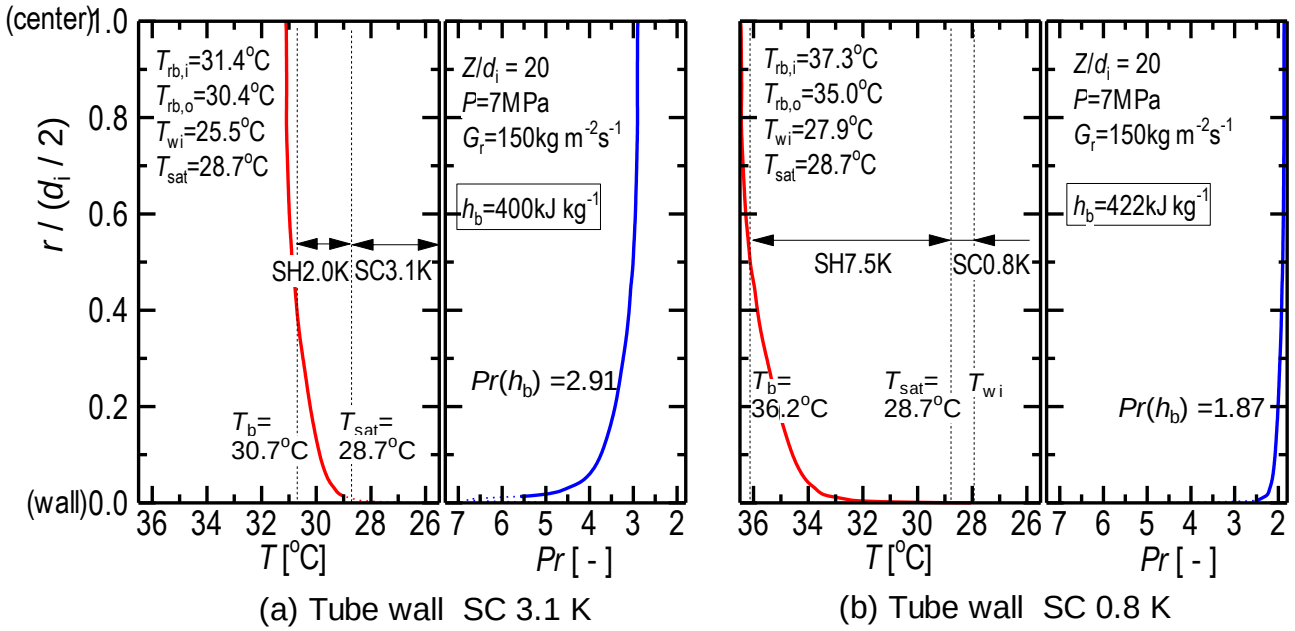

Figure 7 Estimated radial profile of temperature and Prandtl number in radius direction

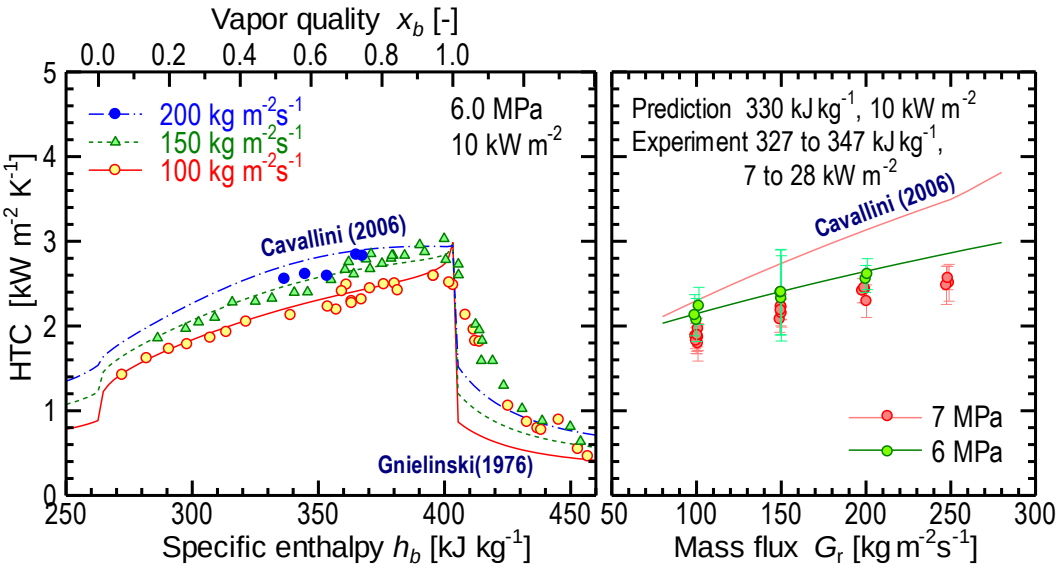

(a) mass flux

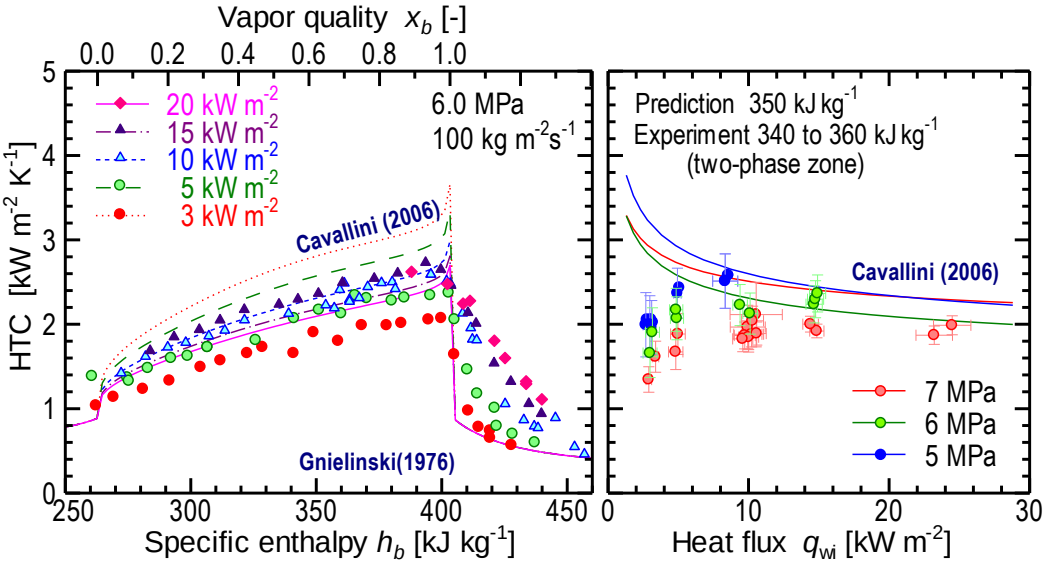

(b) heat flux

Figure 8 Effects of mass flux, and heat flux on HTC

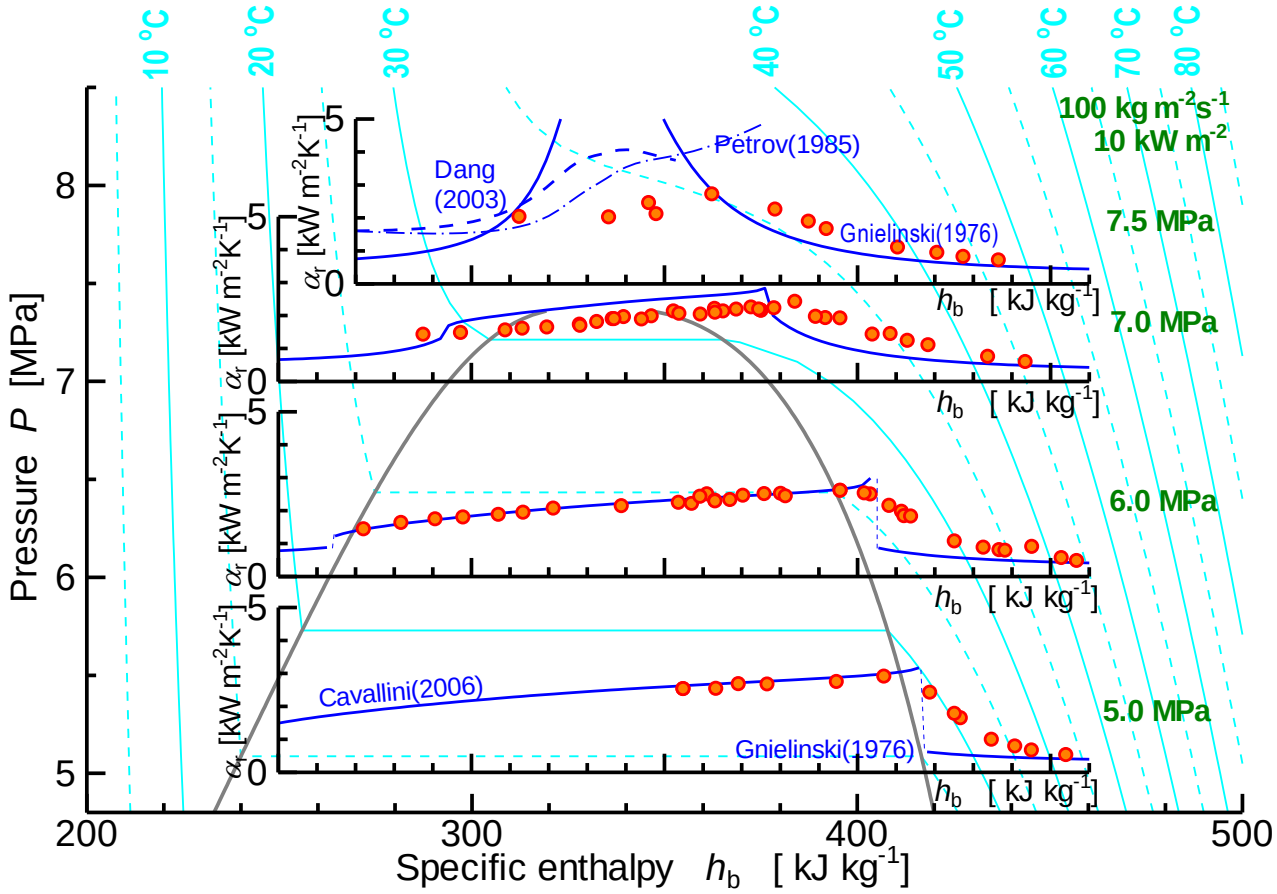

Figure 9 Effect of pressure on HTC

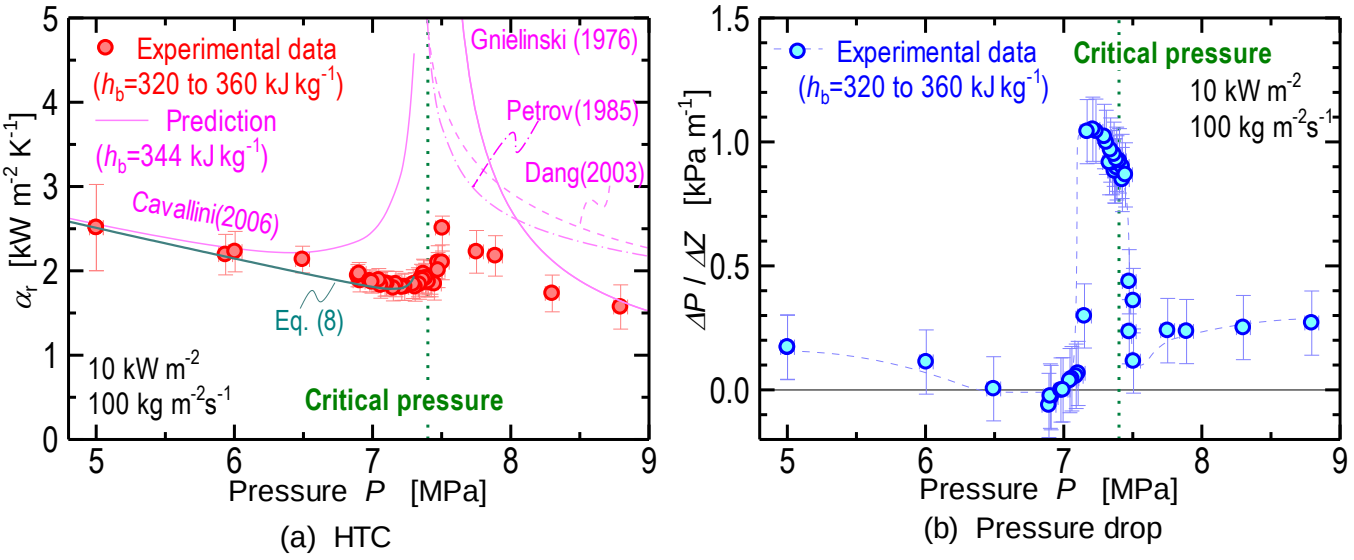

Figure 10 HTC and pressure drop around the critical point

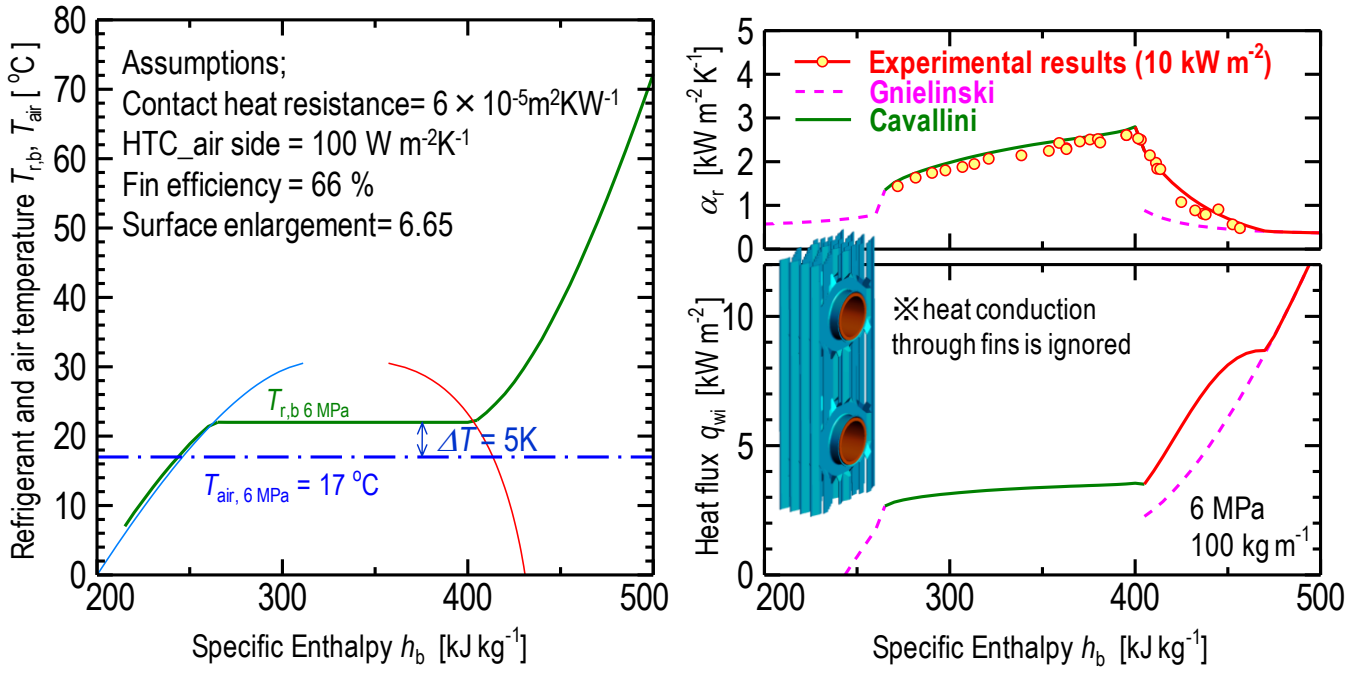

Figure 11 Effect of superheat condensation on cross-finned tube heat exchangers

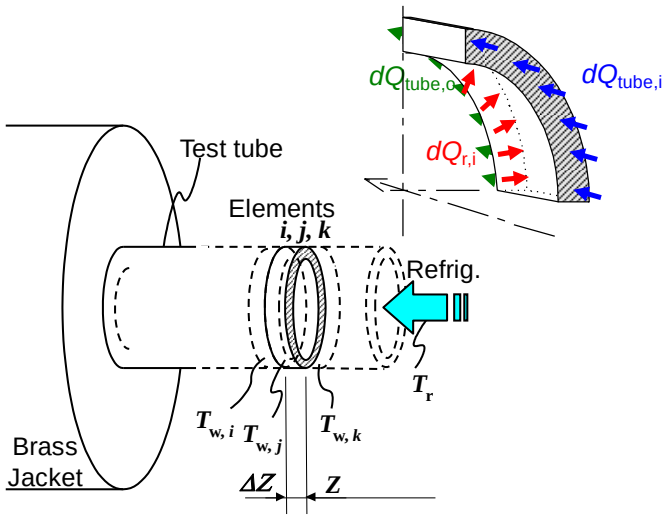

Figure A. 1 Temperature distribution of tube wall and refrigerant

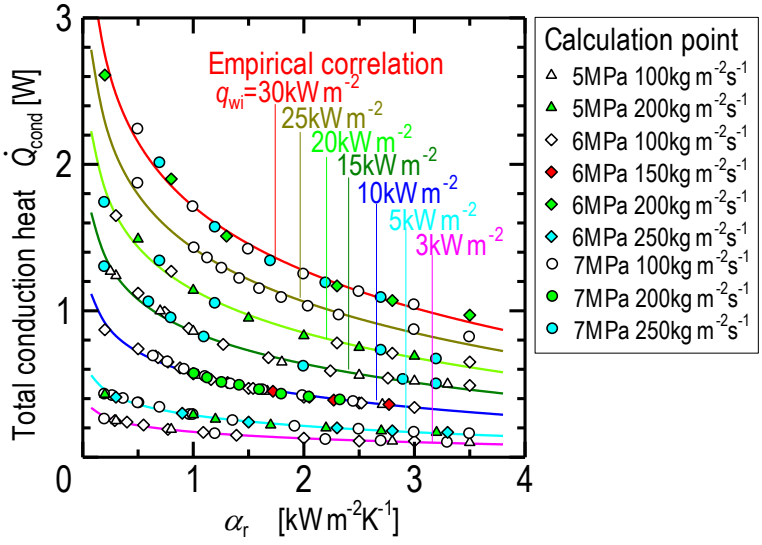

Figure A. 2 Heat conduction from outside the test section

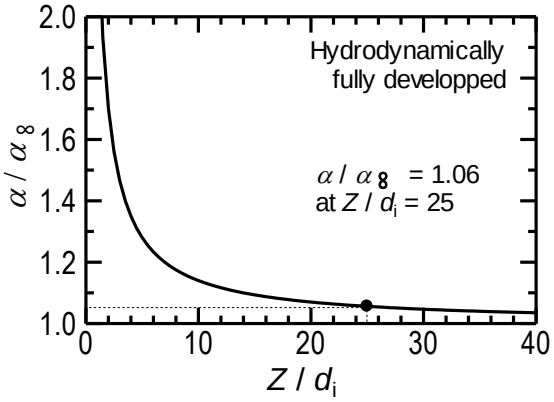

Figure B. 1 Effect of thermal entry length on averaged HTC

Table caption list

Table 1 Test conditions

Inner diameter of the test tube	d_i	6.1 mm
Refrigerant mass flux	G_r	100, 150, 200, 250 kg $m^{-2}s^{-1}$
Pressure	P	5.0, 6.0, 7.0, 7.5 MPa
Averaged heat flux on interior tube wall	q_{wi}	3 to 30 kW m^{-2}
Test section bulk enthalpy	h_{rb}	250 to 480 kJ kg^{-1}

Table 2 Measurement uncertainties

Measurement points		Instrument	Uncertainty
Refrigerant and water temperature	T_{rb}, T_{H2O}	Sheathed thermocouple (T type)	±0.05 K
Tube wall temperature	T_{wi}	Twisted thermocouple (T type)	±0.10 K
Absolute pressure in the mixer	P_{MC}	Absolute pressure transducer	±0.05 MPa
Differential pressure through the test section and pre-cooler	ΔP_{PC}, ΔP_{TS}	Differential pressure transducer	±0.26 kPa
Refrigerant and water mass flow rate of the test section	m_{H2O}, m_r	Coriolis mass flow meter	±0.1 g s^{-1}
Water mass flow rate of the pre-cooler	m_{PC}	Coriolis mass flow meter	±0.5 g s^{-1}

Table 3 Comparative correlations for HTC

Below critical pressure

<Subcool and superheat zone>

$$Nu_b = \frac{\alpha_r d_i}{\lambda_b} = \frac{q_{wi}}{(T_{rb} - T_{wi})}\frac{d_i}{\lambda_b} = Nu_0 F_a \qquad F_a = \begin{cases} (\mu_b/\mu_{wi})^{0.14} & \text{for subcool zone} \\ (T_{wi}/T_{rb})^{-0.36} & \text{for superheat zone} \end{cases}$$

where, F_a is the correction factor for property variation by Sieder-Tate (1936) and Petukhov (1970). Nu_0 is the Nusselt number for constant property, which does not account radial property change, as;

Dittus-Boelter (1930) modified by Colburn(1933): $Nu_0 = 0.023(G_r d_i/\mu_b)^{0.8} Pr_b^{1/3}$

Petukhov (1970) : $Nu_0 = \left[(f_b/8)(G_r d_i/\mu_b) Pr_b\right] \Big/ \left[1.07 + 12.7(f_b/8)^{1/2}\left(Pr_b^{2/3} - 1\right)\right]$

Gnielinski(1976): $Nu_0 = \left[(f_b/8)(G_r d_i/\mu_b - 1000) Pr_b\right] \Big/ \left[1 + 12.7(f_b/8)^{1/2}\left(Pr_b^{2/3} - 1\right)\right]$

where f is Filonenko's friction factor (1954) $f_b = \left[1.82 \cdot \log_{10}(G_r d_i/\mu_b) - 1.64\right]^{-2}$

<Two phase zone>

Haraguchi *et al*. (1994)*:

$$Nu = (\alpha_r d_i/\lambda_L) = \left(Nu_{FC}^{\ 2} + Nu_{BF}^{\ 2}\right)^{1/2}$$

$$Nu_{FC} = 0.0152\left(1 + 0.6 Pr_L^{\ 0.8}\right)(\Phi_V/X_{tt}) Re_L^{\ 0.77}, Nu_{BF} = 0.725 \cdot H(\xi) \cdot (Ga \cdot Pr_L/Ph)^{1/4}$$

$$\Phi_V = 1 + 0.5\left(G_r \Big/ \sqrt{g d_i \rho_V (\rho_L - \rho_V)}\right)^{0.75} X_{tt}^{\ 0.35}, Ga = g\rho_L^{\ 2} d_i^{\ 3}/\mu_L^{\ 2}, Ph = Cp_L (T_{sat} - T_{wi})/h_{LV}$$

$$H(\xi) = \xi + \left\{10\left[(1-\xi)^{0.1} - 1\right] + 1.7 \times 10^{-4} Re_L\right\}\sqrt{\xi}\left(1 - \sqrt{\xi}\right)$$

Cavallini *et al*. (2006)*:

$$J_G = xG_r \Big/ \sqrt{g d_i \rho_V (\rho_L - \rho_V)}, J_G^{\ T} = \left\{\left(7.5/4.3 X_{tt}^{\ 1.111} + 1\right)^{-3} + 2.6^{-3}\right\}^{-1/3}$$

$$\alpha_{LO} = 0.023 Re_{LO}^{\ 0.8} Pr_L^{\ 0.4} \lambda_L / d_i$$

$$\alpha_{strat} = 0.725\left\{1 + 0.741\left(\frac{1-x}{x}\right)^{0.3321}\right\}^{-1}\left[\frac{\lambda_L^{\ 3}\rho_L(\rho_L - \rho_V) g h_{LV}}{\mu_L d_i (T_{wi} - T_{sat})}\right]^{0.25} + \left(1 - x^{0.087}\right) a_{LO}$$

$$\alpha_r = \begin{cases} J_G > J_G^{\ T} : \alpha_A = \alpha_{LO}\left[1 + 1.128 x^{0.8170}(\rho_L/\rho_V)^{0.3685}(\mu_L/\mu_V)^{0.2363}(1 - \mu_V/\mu_L)^{2.144} Pr_L^{\ -0.1}\right] \\ J_G \le J_G^{\ T} : \left[\alpha_A\left(J_G^{\ T}/J_G\right)^{0.8} - \alpha_{strat}\right]\left(J_G/J_G^{\ T}\right) + \alpha_{strat} \end{cases}$$

* Liquid and vapor properties are represented at the saturation temperature in both correlations.

Above critical pressure

Petrov and Popov (1985):

$$Nu_{\mathrm{b,wi}} = \frac{a_{\mathrm{r}} d_{\mathrm{i}}}{\lambda_{\mathrm{wi}}} = \frac{\left(f_{\mathrm{wi}}/8\right)\left(G_{\mathrm{r}} d_{\mathrm{i}}/\mu_{\mathrm{wi}} - 1000\right) Pr_{\mathrm{wi}}}{1.07 + 12.7\left(f_{\mathrm{wi}}/8\right)^{1/2}\left(Pr_{\mathrm{wi}}^{\ 2/3} - 1\right)} \left(1 - 0.001\frac{q_{\mathrm{wi}}}{G_{\mathrm{r}}}\right)\left(\frac{\bar{C}p}{Cp_{\mathrm{wi}}}\right)^{n}$$

$$f_{\mathrm{wi}} = \left[1.82 \cdot \log_{10}\left(G_{\mathrm{r}} d_{\mathrm{i}}/\mu_{\mathrm{wi}}\right) - 1.64\right]^{-2}, \qquad n = \begin{cases} Cp_{\mathrm{wi}} < \bar{C}p : 0.9 - 0.0004\left(q_{\mathrm{wi}}/G_{\mathrm{r}}\right) \\ Cp_{\mathrm{wi}} \geq \bar{C}p : 0.66 - 0.0004\left(q_{\mathrm{wi}}/G_{\mathrm{r}}\right) \end{cases}$$

Dang and Hihara(2003):

$$Nu_{\mathrm{b,f}} = \frac{\alpha_{\mathrm{r}} d_{\mathrm{i}}}{\lambda_{\mathrm{f}}} = \frac{\left(f_{\mathrm{f}}/8\right)\left(G_{\mathrm{r}} d_{\mathrm{i}}/\mu_{\mathrm{b}} - 1000\right) Pr^{*}}{1.07 + 12.7\left(f_{\mathrm{f}}/8\right)^{1/2}\left(Pr^{*2/3} - 1\right)}, Pr^{*} = \begin{cases} Cp_{\mathrm{b}} \leq \bar{C}p : \bar{C}p \cdot \mu_{\mathrm{b}}/\lambda_{\mathrm{b}} \\ Cp_{\mathrm{b}} > \bar{C}p : Cp_{\mathrm{b}} \cdot \mu_{\mathrm{b}}/\lambda_{\mathrm{b}} \end{cases}$$

$$f_{\mathrm{f}} = \left[1.82 \cdot \log_{10}\left(G_{\mathrm{r}} d_{\mathrm{i}}/\mu_{\mathrm{f}}\right) - 1.64\right]^{-2}$$

Table 4 Comparative correlations for pressure drop

Below critical pressure

<Subcool and superheat zone>

Momentum change term in Eq.(7): $\Delta P_{\mathrm{M}} = G_{\mathrm{r}}^{\ 2}\left(\frac{1}{\rho_{\mathrm{b,inlet}}} - \frac{1}{\rho_{\mathrm{b,outlet}}}\right)$

Friction term of Colburn (1933) : $\frac{dP_{\mathrm{F}}}{dZ} = 4 \times 0.046 Re_{\mathrm{b}}^{\ -0.2}\left(\frac{G_{\mathrm{r}}^{\ 2}}{2 d_{\mathrm{i}} \rho_{\mathrm{b}}}\right)$

<Two phase zone>

Momentum change term:

$$\Delta P_{\mathrm{M}} = G_{\mathrm{r}}^{\ 2}\left\{\left[\frac{x^2}{\xi\rho_{\mathrm{V}}} + \frac{\left(1-x\right)^2}{\left(1-\xi\right)\rho_{\mathrm{L}}}\right]_{\mathrm{inlet}} - \left[\frac{x^2}{\xi\rho_{\mathrm{V}}} + \frac{\left(1-x\right)^2}{\left(1-\xi\right)\rho_{\mathrm{L}}}\right]_{\mathrm{ontlet}}\right\}$$

Friction term of Friedel(1979)**:

$$\left(\frac{dP_{\mathrm{F}}}{dZ}\right) = \Phi_{\mathrm{LO}}^{\ 2} \cdot 4 \times 0.0791 Re_{\mathrm{LO}}^{\ -0.25}\left(\frac{G_{\mathrm{r}}^{\ 2}}{2 d_{\mathrm{i}} \rho_{\mathrm{L}}}\right)$$

$$\Phi_{\mathrm{LO}}^{\ 2} = C_{\mathrm{F1}} + \frac{3.24 C_{\mathrm{F2}}}{Fr_{\mathrm{h}}^{\ 0.045} We_{\mathrm{L}}^{\ 0.035}}, Fr_{\mathrm{h}} = \frac{G_{\mathrm{r}}}{g d_{\mathrm{i}} \rho_{\mathrm{h}}}, \quad We_{\mathrm{L}} = \frac{G_{\mathrm{r}}^{\ 2} d_{\mathrm{i}}}{\sigma \rho_{\mathrm{h}}}, \quad \rho_{\mathrm{h}} = \left(\frac{x}{\rho_{\mathrm{V}}} + \frac{1-x}{\rho_{\mathrm{L}}}\right)^{-1}$$

$$C_{\mathrm{F1}} = \left(1-x\right)^2 + x^2\left(\rho_{\mathrm{L}}/\rho_{\mathrm{V}}\right)\left(\mu_{\mathrm{V}}/\mu_{\mathrm{L}}\right)^{0.25}$$

$$C_{\mathrm{F2}} = x^{0.78}\left(1-x\right)^{0.224}\left(\rho_{\mathrm{L}}/\rho_{\mathrm{V}}\right)^{0.91}\left(\mu_{\mathrm{V}}/\mu_{\mathrm{L}}\right)^{0.19}\left(1-\mu_{\mathrm{V}}/\mu_{\mathrm{L}}\right)^{0.7}$$

** Liquid and vapor properties are represented at the saturation temperature in this correlation.